Dynamic Article Links ►

Cite this: DOI: 10.1039/c0xx00000x

www.rsc.org/xxxxxx

ARTICLE TYPE

Uniform Porous Multilayer-Junction Thin Film for Enhanced Gas-Sensing Performance

Ping-Ping Zhang, Hui-Zhang, Xu-Hui Sun*

Received (in XXX, XXX) Xth XXXXXXXXX 20XX, Accepted Xth XXXXXXXXX 20XX
DOI: 10.1039/b000000x

Highly-uniform In_2O_3/CuO bilayer and multilayer porous thin films were successfully fabricated using self-assembled soft template and simple sputtering deposition technique. The sensor based on the In_2O_3/CuO bilayer porous thin film shows obviously improved sensing performance to ethanol at the lower working temperature, compared to single layer counterpart sensors. The response of In_2O_3/CuO bilayer sensors exhibit nearly 3 and 5 times higher than those of the single layer In_2O_3 and CuO porous film sensors over the same ethanol concentration, respectively. The sensing mechanism based on p-n hetero-junction, which contributed to the enhanced sensing performance was also experimentally confirmed by a control experiment which the SiO_2 insulation layer was inserted between the In_2O_3 and CuO layers to break the p-n junction. In addition, the sensing performance can be further enhanced by increasing the number of In_2O_3/CuO junction layers. The facile process can be easily extended to the fabrication of other semiconductor oxide gas sensors for practical sensing applications.

Introduction

With the progress of solid-state semiconductor chemical sensors being widely used to detect toxic gases, gas sensors based on metal oxide semiconductor (MOS), such as In_2O_3[1, 2], ZnO[3], SnO_2[4], TiO_2[5] and CuO[6], etc., are the most promising candidates due to their low power consumption, high sensitivity and satisfactory selectivity, low detection limit, simplicity in fabrication and manipulation, high compatibility with microelectronic processing[7, 8]. It is well-known that the gas sensing characteristics are greatly dependent on its morphology and structure, such as porosity, grain size, surface-to-volume ratio and shape which effect gas adsorption and the change of the conductivity caused by the surface interaction process between materials and the gas molecules[9-12]. For example, increased surface area can improve the response performance. Hence, one of the efficient strategy to improve the sensing capability is to use nanostructured materials for sensing materials, such as nanoparticles[13], nanorods[3], nanotubes[14], nanobelts[15], nanowires[16], nanoporous[17], nanosheets[18], etc., due to their structural diversity and a large surface area with which gas molecules can interact more, consequently producing sensing performances superior to their film or bulk counterparts. Among various types of the nanostructured sensing materials, ordered nano/micro porous materials, in particular, have elicited much interest as a favorable candidate recently because of their high surface area/volume ratio and regular morphology which are advantageous to accomplish not only high gas sensitivity and rapid response, but also good reproducibility. Many previous papers have reported the porous structured sensing materials obtained by various methods, such as wet chemical methods[19, 20] (mainly sol−gel process), resulting in high sensitivity and reasonable stability. However, the pore size, porosity and the film thickness cannot be well controlled, resulting in the uncontrollability and irreproducibility of the sensing performance, which is unfavorable for the practical application of the sensing elements[21]. Recently, we have been developed a facile approach to fabricate well-ordered porous films, with homogeneous and controlled film thickness and the controllable pore sizes, on Si substrates and the initial findings and early results of this promising approach were presented[17]. It is worth noting that the response time and the sensitivity of such porous MOS films sensors can be enhanced by metal doping using co-sputtering.

It is well known that, in addition to the material characteristics, hetero-structure[22], based on a unique sensing mechanism, has already been proved to result in the improvement of the sensing performances compared to their single-component semiconductor gas sensors due to the synergetic effect from different sensing materials in the hetero-structure and the hetero-junction barrier formed at the interfaces. Previously, various types of hetero-structures including hetero-junction nanocrystals[23], hetero-junction nanowires[24], and hetero-junction arrays[25] have been synthesized. Hetero-junction nanomaterials with multi-layer structure have multi-barrier structures which lead to periodic accumulation of carriers and control of their transport properties[22]. In continuation of our efforts the present investigation reported herein describes in detail our successful attempts towards obtaining simple formation of porous multilayer hetero-junction thin film thereby creating p-n hetero-junctions by simple soft template and sputter deposition process. The multilayer porous structure fabricated by the soft template combining with sol-gel method is also hard to get the multilayer hetero-junctions porous films[26,27,28]. Different from these previous reported hetero-junction materials, the porous multilayer hetero-junctions films fabricated by this method can be considered as a vertical hetero-junction pattern. Nowadays, it is still hard to synthesize vertical-multi-layer hetero-structure with strictly periodic arrangement using traditional methods, such as sol-gel method[20, 29]. In this study, we demonstrate a facile method to fabricate the well-ordered bilayer and multilayer porous thin film via combining a self-assembly of polystyrene spheres as a soft template with the RF sputter deposition. As a sample, the In_2O_3/CuO bilayer and multilayer porous thin film has been successfully fabricated for ethanol detection. P-type CuO[30], and n-type In_2O_3[31], have been widely chosen as sensing materials, especially their corresponding nanoscale counterparts[32, 33], such as nanowire[34, 35], nanorods[30], nanoparticle[36], and nanostructured film[37], for ethanol sensing applications. We found that the In_2O_3/CuO p-n hetero-junction porous film, which is well-ordered vertical multilayer film with strictly periodic structure, is much efficient to the ethanol detection with much higher sensitivity, selectivity and lower temperature than that of pure In_2O_3 and CuO thin porous film alone.

Experimental section

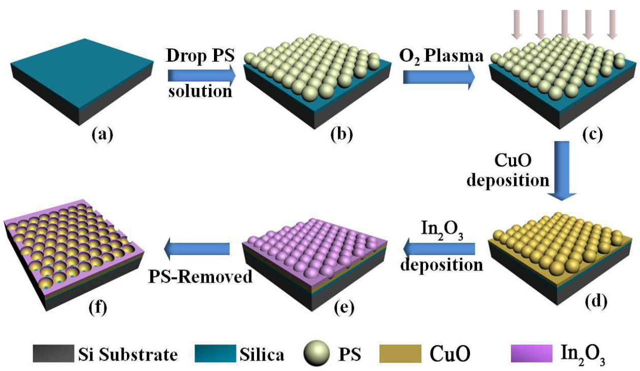

Fig. 1 the schematic of the side view of uniform In_2O_3/CuO bilayer porous thin film.

The fabrication process of single and multilayer metal oxides porous thin films is shown in Fig. 1. Briefly, the ordinary silicon with 200 nm silicon dioxide layer (SiO_2/Si) substrate was ultrasonically cleaned in acetone, ethanol and distilled water, respectively, and then treated by O_2 plasma to obtain a completely hydrophilic surface as before[17]. After cleaning, an aqueous suspension of polystyrene (PS) beads (2 wt%) of approximately 500 nm in diameter was spin-coated on the SiO_2/Si substrate and dried in air at room temperature to obtain a monolayer self-assembly of PS beads. To adjust the pore size, the isotropic plasma etching of the PS beads was performed by a reaction ion etching (RIE) system (Oxford plasma lab 80 plus) for 1-2 minutes with approximately 40 sccm gas flow O_2 at 275 mtorr pressure and RF 90 W power. Afterwards, the In_2O_3 and CuO films were deposited upon the substrate covered with uniform close-packed PS monolayer in a radio-frequency power supply magnetron sputtering system (PVD 75, Kurt J Lesker) at room temperature using In_2O_3 and CuO targets, respectively. The multilayer In_2O_3/CuO films were obtained by sputtering these two materials in turn. After the deposition, the samples were subjected to an ultrasound treatment in toluene to wash out the PS beads and then calcined at 500 °C for 4 h to crystallize the films, resulting in the formation of thin films with closed-linked hollow pores on the substrate. In order to fabricate gas sensors, the interdigital electrodes was deposited on the surface of the periodic pore array thin film by the electron-beam evaporation deposition system (PVD 75, Kurt J Lesker) at a background pressure of 7×10^{-6} torr with Au (100 nm)/Ti (5nm) electrodes (finger spacing: 150 µm, 3.4 mm in length, 200 µm in width) as shown in figure S1a. The Si substrate with SiO_2 layer is covered with the bilyer porous thin film indicates formation of a periodic pore array.

Surface morphologies and microstructures of the as-prepared porous films were characterized by scanning electron microscopy (SEM, FEI Co., model Quanta-200) and atomic force microscopy (AFM) (Multimode V system, Veeco) using a tapping mode. The crystal structure identification of the porous thin films were performed by X-ray diffraction (XRD, Empyrean, PANalytical, Holland), using a Philips X'pert PRO MPD diffractometer with Cu Kα radiation (λ= 0.15406 nm) in the 2θ range of 15-80°. The chemical composition and chemical state of these samples were studied by X-ray photoelectron spectroscopy (XPS, Kratos AXIS UltraDLD).

Gas-sensing properties were measured using a home-built intelligent gas sensing analysis system. This sensor system consist of a vacuum stainless steel chamber (about 2L in volume) equipped with appropriate gas inlets and outlets, sensor holder, heating plate, a pair of electrodes, vacuum pump, Keithley sourcemeter-2400, mass flow controllers and data acquisition system shown in Fig. S1a. A DC power supply was connected to the heating plate to control the working temperature of sensors, which can offer a substrate temperature control (from room temperature to 500 °C). Dry air was used as the carrier gas and the diluting gas to obtain desired concentrations of target gases. The gas-sensing properties were measured in a dynamic condition, in which the carrier gas and the given amount of the C_2H_5OH gas continuously flowed through the sensing chamber. I-V characteristics of the sensors were measured by a computer-controlled Keithley-2400 system. The sensor resistance and sensitivity were collected and analyzed by the system in real time. The gas sensitivity (S) was defined as the ratio of their resistances in air (Ra) to those in a mixed of target gases (Rg), in which the S is Ra/Rg for n-type semiconductor and the S is Rg/Ra for p-type semiconductor. Response and recovery times was defined as the time taken by the sensors to achieve 90% of total resistance change during either the adsorption or the desorption process, respectively.

Results and discussion

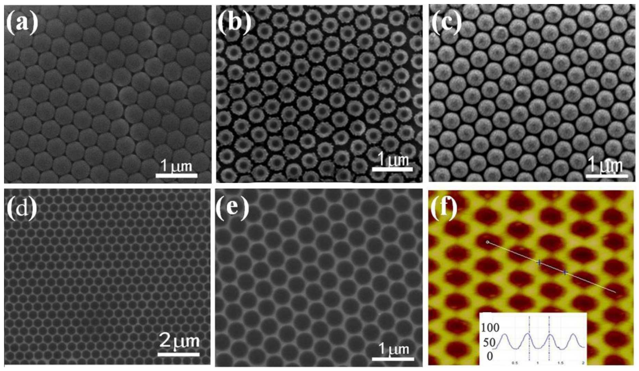

Fig. 2 SEM images of self-assemble PS template (a), PS template after plasma etching (b), etched PS template after magnetron sputter deposition (c) and after ultrasonic washing (d) (e), AFM image of In_2O_3/CuO bilayer porous thin film (f).

The large-area well-ordered single and multilayer porous thin films were fabricated on a SiO_2/Si substrate successfully, as illustrated in Fig. 1. The morphology of the PS temple and as-prepared In_2O_3/CuO bilayer porous thin film on the substrate were characterized using SEM and AFM as shown in Fig. 2. The as-prepared self-assembled monolayer PS with the diameter of 500 nm is uniform and the spherical PS beads take on hexagonal close-packed structure and contact with each other by quasi-point style. Correspondingly, the interstices among the close-packed PS microspheres suffered oxygen etching become larger to the desirable size from top view SEM image shown in Fig. 2(b). During this RIE process, the dimension of PS microspheres can be easily controlled by adjusting the etching time and further determine the pore size of the thin film. Fig. 2(c) shows the self-assembled PS temple after In_2O_3 (40 nm) and CuO (40 nm) films deposition. The metal oxide layer fills the interspacing of the PS template with the hexagonal structure. Before the PS template removal, the metal oxide thin film on the surface of the PS template look likes the opal structure shown in Fig. 2(c). While, after the PS template washed by toluene, the PS template with the metal oxide was washed away, then the honey comb liked structure was formed seen in Fig. 2(d). Figs. 2(d)-(e) show SEM images of the as-prepared bilayer In_2O_3/CuO porous thin film after the PS temple removal. The as-prepared In_2O_3/CuO porous thin film is uniform at large scale. The ordered porous film is honeycomb-like in morphology and all the spherical pores are hexagonally arranged. The thickness and pore diameter of bilayer In_2O_3/CuO porous thin film are 80 nm and 450 nm, respectively, obtained from the AFM image in Fig. 2(f).

XRD experiment was conducted to determine the crystal structure of the porous thin films. The XRD patterns of the as-synthesized bilayer In_2O_3/CuO compared with the pure In_2O_3 and CuO single layer after the annealing treatment are shown in Fig. S1†. The well-defined diffraction peaks in the spectra of the pure In_2O_3 and CuO porous film can be both indexed to cubic phase In_2O_3 (JCPDS Card No. 89-4595) and cubic phase CuO (JCPDS Card No. 89-2530), respectively. The XRD data indicate that the pure In_2O_3 and CuO porous films are crystalline after the annealing treatment in air at 500 °C. Meanwhile, all the peaks in the XRD pattern of the In_2O_3/CuO bilayer porous thin film suggest that both the top layer In_2O_3 film and the bottom layer CuO film are crystalline as well, which are mainly originated from cubic In_2O_3 and CuO layer with separate phases. It is easily found that there are no obvious peak shifts or any trace of other phases besides cubic In_2O_3 and CuO.

XPS studies were carried out to further investigate chemical states of constituent elements of the as-prepared In_2O_3/CuO bilayer porous film. The XPS spectra of In 3d and Cu 2p are illustrated in Fig. S2†. Fig. S2(a)† displays two peaks at the binding energies of 444.6 eV and 452.1 eV, corresponding to In $3d_{5/2}$ and In $3d_{3/2}$, respectively, with the values In^{3+} in In_2O_3[38]. The core level Cu 2p spectrum of In_2O_3/CuO bilayer porous film displayed in Fig. S2(b)† shows the similar feature as that of Cu in CuO and the observed binding energy at 933.5 eV and 953.6 eV, assigned to Cu $2p_{3/2}$ and Cu $2p_{1/2}$ bands, respectively, is consistent with the value for Cu in CuO[39]. In addition, the clear shake-up feature around 940-945 eV further suggests that CuO is present[40]. The XPS results further clarify the bilayer porous thin film is the presence of In_2O_3 and CuO, respectively. Both XRD and XPS results provide the insight that the surface state of the In_2O_3 and CuO layer in the In_2O_3/CuO bilayer porous thin film has not been changed significantly while the p-n junction is formed.

The gas sensing properties of In_2O_3/CuO bilayer porous film sensor and single layer In_2O_3 and CuO porous film sensors toward ethanol gas were systemically studied and compared in Fig. 3. Fig. 3(a) exhibits the responses of three different sensors to 1000 ppm ethanol as a function of operating temperature. All these sensors have the same evolution trend: the responses first increase with elevated temperature, up to an optimal working temperature and then gradually decrease with continuous increase of temperature. Among them, the bilayer porous film sensor demonstrates considerably the lowest optimum working temperature, which is 250 °C compared to single layer porous film sensors with 300 °C and 350 °C for pure In_2O_3 and CuO porous film, respectively. Also, the sensitivity of the In_2O_3/CuO bilayer porous film sensor is higher than those of pure In_2O_3 and CuO porous film gas sensors. For example, the sensitivity of the In_2O_3/CuO bilayer sensor toward 1000 ppm ethanol at 250 °C is estimated to be 9.6, which is much higher than those of other two single layer sensors, 3.8 and 1.9 for the pure In_2O_3 and CuO sensors, respectively. In addition, the sensitivity of the bilayer porous film sensor still reaches an acceptable value (1.7) toward 1000 ppm ethanol gas even under the room temperature. We suggest that the p-n junction was formed between the In_2O_3/CuO bilayer, which leads to the decrease of activation energy of the bilayer sensor and further results in decrease of optimum working temperature for the gas sensing response and the improved sensing performance.

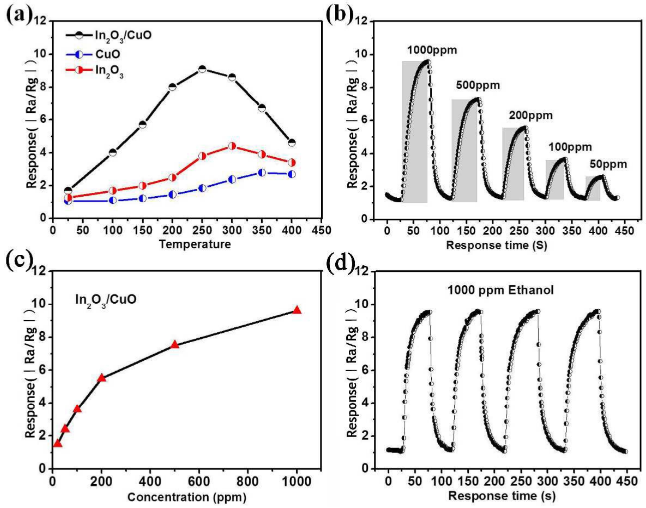

Fig. 3 (a) Response of different sensing materials to 1000 ppm ethanol at different temperature, (b) the response of In_2O_3/CuO bilayer porous film to ethanol of different concentration ranging from 50 ppm to 1000 ppm at 250 °C, (c) the sensitivity of In_2O_3/CuO bilayer porous thin film on the concentrations of ethanol varying from 20 ppm to 1000 ppm at 250 °C, (d) the response of In_2O_3/CuO bilayer porous thin film to 1000 ppm ethanol at 250 °C under 4 cycles.

To obtain a deep insight into the gas sensing behavior of In_2O_3/CuO bilayer film sensor, the dynamic sensing transient of the In_2O_3/CuO bilayer gas sensor exposed to ethanol in the range of 50-1000 ppm at 250 °C is shown in Fig. 3(b). It is apparent that the sensor responds rapidly with the exposure in ethanol mixture gas and recovers quickly to baseline after the exposure to air again. The response and recovery times are determined to be 48 s and 30 s, respectively. Furthermore, the response of the sensor to ethanol increases with the increase of the ethanol concentration. The In_2O_3/CuO bilayer sensor still shows an acceptable response (2.7) from the view of the practical application when the ethanol concentration is down to 50 ppm. The dependence of response as a function of ethanol concentration for the In_2O_3/CuO bilayer porous thin film was shown in Fig. 3(c). It can be observed that the response increases rapidly with increasing ethanol concentration below 200 ppm at a linear relationship and the sensor shows a slow growth with further increasing the ethanol concentration ranging from 200-1000 ppm, indicating that the sensor becomes more or less saturated. Therefore, the applicability of the sensor for the concentration detection in the real field application can be realized, especially in the low concentration range.The response transient cycles of the In_2O_3/CuO bilayer porous film sensor to 1000 ppm ethanol were evaluated at 250 °C. The reversible cycles of the response curve indicate a stable and repeatable response characteristic as shown in Fig. 3(d).

Fig. 4 shows the selectivity of the In_2O_3/CuO bilayer porous thin film compared with the pure In_2O_3 and CuO porous film gas sensors to 1000 ppm ethanol, methanol, acetone, NH_3 and CO at 250 °C. It should be highlighted that the In_2O_3/CuO bilayer sensor has excellent selectivity to ethanol while exhibit very weak to the other typical interference gases. However, the pure In_2O_3 and CuO porous thin films show the lower sensitivity and selectivity to all of this detect gases.

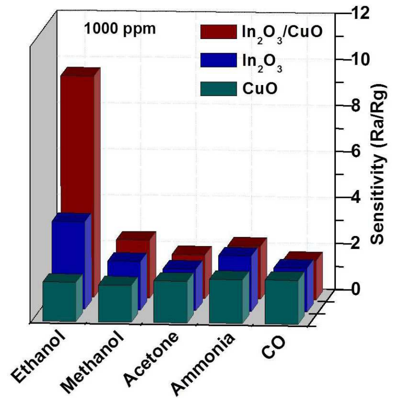

Fig. 4 Sensitivity of In_2O_3, CuO single layer porous film and In_2O_3/CuO bilayer porous thin film to 1000 ppm different gases at 250 °C.

The as-prepared sensor based on the In_2O_3/CuO bilayer porous thin film shows the higher response and better selectivity to ethanol and the lower detection temperature, compared to those of pure single layer porous film sensors, which may be attributed to the effect of p-n junction formed between the interface of In_2O_3 and CuO layers. The In_2O_3 and CuO of the In_2O_3/CuO bilayer film are n-type and p-type semiconductor oxides, respectively, and the sensing mechanism of the In_2O_3/CuO bilayer film is based on a surface reaction with the adsorption and desorption of the gas molecules on the surface of the sensing materials, which can cause the change in resistance in air and in ethanol[41]. Thus, we suggests that the p-n junction was formed at the interfaces of the In_2O_3/CuO film in which the adsorption was enhanced, taking contributions to the enhanced sensitivity and good selectivity of detecting ethanol at the lower working temperature. The current–voltage characteristics for the sensors based on In_2O3, CuO and In_2O_3/CuO porous thin film was also displayed seen in Fig. S4. As shown in Fig. 4S, all sensors show current–voltage linear relationships in the operating range of voltage and current, clearly indicating that good ohmic contacts between the porous structured materials and the electrode layers were formed. Further, the In_2O_3/CuO porous thin film is observed to possess higher resistance compared to In_2O_3 and CuO porous thin film. The large resistance increase of In_2O_3/CuO demonstrated that p-n hetero-junction was successfully formed.

The above sensing performance results demonstrate that ethanol sensing mechanism on In_2O_3/CuO hybrid is different from that of pure materials, which is due to the formation of p-n hetero-junctions. The enhanced gas performance for the In_2O_3/CuO bilayer porous thin film sensor can be interpreted using a schematic diagram of the energy band structure at thermal equilibrium and the sensing mechanism schematic model of In_2O_3/CuO p–n hetero-junction as shown in Fig. 6. As shown in figure 6a, EF is the Fermi level; Ev and Ec are the valence band and conduction band, respectively. For this hetero-junction structure, CuO is p-type and In_2O_3 is n-type semiconductor. By combining the In_2O_3 and CuO thin film, p–n hetero-junction is formed at the interface between these two different types of metal oxide. Then, the electrons transfer from n-type In_2O_3 to p-type CuO while the holes transfer from CuO to In_2O_3 until the system obtains equalization at the Fermi level, and a wide electron depletion layer will be generated at the hetero-junction interface, which resulting in band bending as shown in figure 6a. The charges existed on the In_2O_3/CuO surface of the p-n hetero-junction, resulting in the ability of In_2O_3/CuO nanostructures to attract ethanol vapor and oxidative gas O_2 more easily[42, 43, 44].

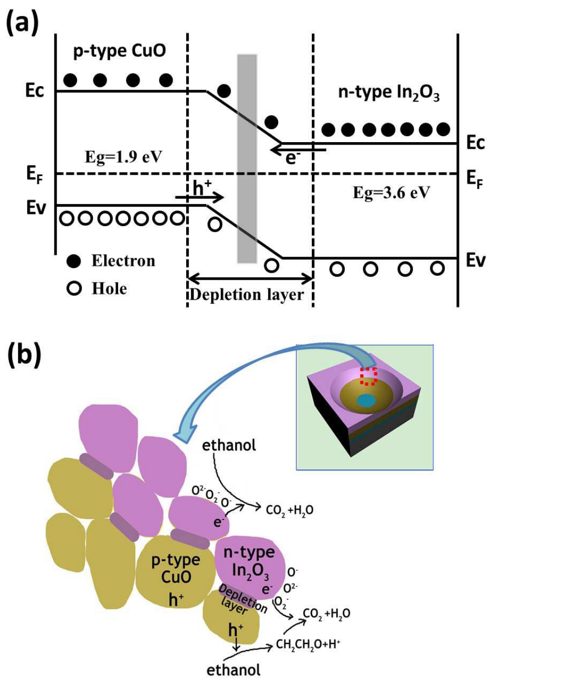

Fig. 5 the schematic energy band diagram of the p-CuO/n-In_2O_3 hetero-junction at thermal equilibrium and the sensing mechanism schematic model for the p-CuO/n-In_2O_3 based sensor when it exposures to ethanol gas

Schematic model for the In_2O_3/CuO based sensor when it exposures to ethanol gas is displayed in Fig. 6 b. As shown in Fig. 6 b, the surface adsorbed C_2H_5OH reacted with the adsorbed oxygen species on the In_2O_3 surface leading to the electrons back to the semiconductor. The In_2O_3/CuO hetero-junction active sites convert C_2H_5OH with O^- (O^{2-}/O_2^-) to CH_3CHO and H_2O (Eq. (1) and (2)).

$$C_2H_5OH + O^-(O^{2-}/O_2^-) \longrightarrow CH_3CHO + H_2O + e^- \qquad (1)$$

$$C_2H_5OH + O^-(O^{2-}/O_2^-) \longrightarrow CO_2 + H_2O + e^- \qquad (2)$$

Meanwhile, the reductive ethanol molecule may combine with the holes in CuO and produces the intermediates CH_3CHO which will react with absorbed oxygen on the n-type In_2O_3 (Eqs. (3) and (4)) at the interface of hetero-junction bilayer film.

$$C_2H_5OH + h^+ + O^-(O^{2-}/O_2^-) \longrightarrow CH_3CHO + H_2O \qquad (3)$$

$$C_2H_5OH + h^+ + O^-(O^{2-}/O_2^-) \longrightarrow CO_2 + H_2O + e^- \qquad (4)$$

Overall, the interface of In_2O_3/CuO p-n hetero-junction easily attract reductive and oxidative gases (O_2), thus forming a deeper electron depletion layer and causing a much higher sensing response than pristine oxides.

In order to further confirm this hypothesis, the 20 nm SiO_2 insulation layer was inserted into the In_2O_3/CuO bilayer porous thin film between the In_2O_3 and the CuO layer film to break the junction as a control sample, as schemed in Fig. 5(a). The SiO_2 insulation layer can prevent the formation of p-n hetero-junctions between the In_2O_3 and the CuO film. For comparison, the sensors response of the In_2O_3/CuO bilayer porous film and the In_2O_3/CuO with the SiO_2 insulation layer porous film (In_2O_3/SiO_2/CuO) were measured under the same conditions as shown in Fig. 5(b). The In_2O_3/SiO_2/CuO porous film sensor exhibits very weak response to 1000 ppm ethanol at the working temperature ranging from 25 °C to 400 °C compared to the In_2O_3/CuO bilayer porous film sensor. The highest response of In_2O_3/SiO_2/CuO sensor is only about 3.5 at 350 °C, which is much lower than that of In_2O_3/CuO sensor (9.6 at 250 °C). In order to further compared the gas response of these sensors, the dynamic gas response curves of the In_2O_3, CuO, In_2O_3/CuO, and In_2O_3/SiO_2/CuO gas sensors to different concentrations (50-1000 ppm) of ethanol are shown in Fig. S4. As depicted, the responses of the entire sensors exhibit drastic rise upon the injection of ethanol gas and quick drop to their initial states after the sensors are exposed to air. Similar to the response results of the mentioned above, In_2O_3/CuO based sensor exhibits the highest responses of different concentration ethanol.

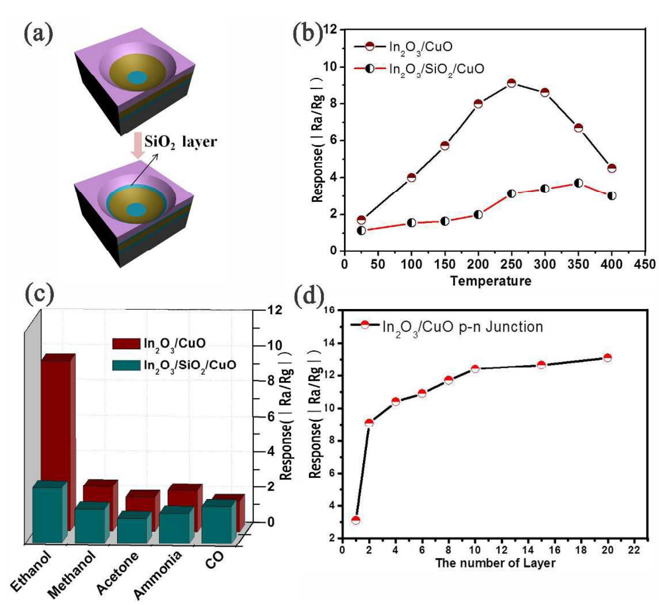

Fig. 6 (a) the schematic illustration of the In_2O_3/CuO bilayer porous thin film before insert the insulation layer and after insert the insulation layer, (b) Response of the In_2O_3/CuO and In_2O_3/SiO_2/CuO based sensors to 1000 ppm ethanol at different temperature, (c) Sensitivity comparison of the In_2O_3/CuO and In_2O_3/SiO_2/CuO based sensors to different 1000 ppm gases at250 °C, (d) Response of gas sensors with different layers to1000 ppm ethanol at 250 °C.

The selectivity of the $In_2O_3/SiO_2/CuO$ sensor compared with the In_2O_3/CuO gas sensor to ethanol with interference gases (methanol, acetone, NH_3, and CO at 1000 ppm) was also investigated under the same condition, and the response to different gases is shown in Fig. 5(c). It can be seen that the $In_2O_3/SiO_2/CuO$ sensor exhibits negligible responses to all the gases and also shows very low selectivity toward the ethanol gas. We further investigated the effect of the number of the p-n junction layers on the performance of the sensors. Fig. 5(d) presents the effect of the number of In_2O_3/CuO junction layers on the response of the sensors to 1000 ppm ethanol. It is clear that the more hetero-junction interfaces, the better sensitivity of the sensors. It was further demonstrated that the p-n junction interfaces acting as the active sites with a wider space charge layer was the key factor which enhanced the sensitivity and selectivity of the In_2O_3/CuO sensor to ethanol. So, the magnitude of the space charge layer by the p-n junctions formed at the interface is determined by the number of the p-n junctions. With the number of the multilayer of the thin film increases, the total thickness of depleted layer increases, inducing more active sites of CuO-In_2O_3 interfaces. When the multilayer sample are made up of more p-n junctions, the change in resistance cause by reaction of ethanol molecules with the chemisorbed surface oxygen species will become greater, thereby meaning a better sensing performance. Therefore, the higher response to ethanol can be simply achieved by increasing the number of layers of the p-n junction sensing materials in our work.

Conclusions

In summary, highly uniform In_2O_3/CuO bilayer and multilayer porous thin films were successfully fabricated using self-assembled soft template and simple sputtering deposition. The sensor based on the In_2O_3/CuO bilayer porous thin film showed obviously improved sensing performance to ethanol at the lower working temperature compared to those of the pristine In_2O_3 and CuO porous film sensors over the same conditions, which could be attributed to the p-n hetero-junction formed between the In_2O_3 and CuO films interface. The p-n hetero-junction mechanism which contributes to the enhanced sensing performance including a high sensitivity and selectivity was experimentally confirmed by the control experiment. Furthermore, the multilayer In_2O_3/CuO sensor showed better responses to ethanol and the sensing performance can be easily enhanced by increasing the number of junction layers. The facile process developed here can be easily extended to the fabrication of other semiconductor oxide gas sensors for practical sensing applications.

Acknowledgements

The work was supported by the National Basic Research Program of China (973 Program) (Grant No. 2010CB934500), Natural Science Foundation of China (NSFC) (Grant No. 91333112), the Priority Academic Program Development of Jiangsu Higher Education Institutions. This is also a project supported by the Fund for Innovative Research Teams of Jiangsu Higher Education Institutions.

Notes and references

Institute of Functional Nano & Soft Materials (FUNSOM), Soochow University, Suzhou, Jiangsu 215123, P. R. China
**E-mail：*xhsun@suda.edu.cn

† Electronic Supplementary Information (ESI) available: XRD spectra of typical In_2O_3/CuO bilayer porous thin film, XPS spectrum of In_2O_3/CuO bilayer porous thin film. See DOI: XXXXXXXX

1 D. H. Zhang, Z. Q. Liu, C. Li, T. Tang, X. L. Liu, S. Han, B. Lei, and C. W. Zhou, *Nano Letters*, 2004, **4**, 10.
2 T. Zhang, F. B. Gu, D. M. Han, Z. H. Wang, and G. S. Guo, *Sensors and Actuators B-Chemical*, 2013, **177**.
3 L. W. Wang, Y. F. Kang, X. H. Liu, S. M. Zhang, W. P. Huang, and S. R. Wang, *Sensors and Actuators B-Chemical*, 2012, **162**, 1.
4 A. A. Firooz, A. R. Mahjoub, and A. A. Khodadadi, *Sensors and Actuators B-Chemical*, 2009, **141**, 1.
5 M. Alexander, and K. Pandian, *Journal of Solid State Electrochemistry*, 2013, **17**, 8.
6 M. Faisal, S. B. Khan, M. M. Rahman, A. Jamal, and A. Umar, *Materials Letters*, 2011, **65**, 9.
7 D. P. Volanti, A. A. Felix, M. O. Orlandi, G. Whitfield, D. J. Yang, E. Longo, H. L. Tuller, and J. A. Varela, *Advanced Functional Materials*, 2013, **23**, 14.
8 C. S. Xie, L. Q. Xiao, M. L. Hu, Z. K. Bai, X. P. Xia, and D. W. Zeng, *Sensors and Actuators B-Chemical*, 2010, **145**, 1.
9 Y. Shimizu, and M. Egashira, *Mrs Bulletin*, 1999, **24**, 6.
10 X. J. Huang, and Y. K. Choi, *Sensors and Actuators B-Chemical*, 2007, **122**, 2.
11 N. Yamazoe, *Sensors and Actuators B-Chemical*, 1991, **5**, 1.
12 J. Rockenberger, E. C. Scher, and A. P. Alivisatos, *Journal of the American Chemical Society*, 1999, **121**, 49.
13 K. Soulantica, L. Erades, M. Sauvan, F. Senocq, A. Maisonnat, and B. Chaudret, *Advanced Functional Materials*, 2003, **13**, 7.
14 O. K. Varghese, D. W. Gong, M. Paulose, K. G. Ong, E. C. Dickey, and C. A. Grimes, *Advanced Materials*, 2003, **15**, 7.
15 E. Comini, G. Faglia, G. Sberveglieri, Z. W. Pan, and Z. L. Wang, *Applied Physics Letters*, 2002, **81**, 10.
16 J. H. Park, and J. H. Lee, *Sensors and Actuators B-Chemical*, 2009, **136**, 1.
17 S. M. Zhang, P. P. Zhang, Y. Wang, Y. Y. Ma, J. Zhong, and X. H. Sun, *Acs Applied Materials & Interfaces*, 2014, **6**, 17.
18 C. S. Moon, H. R. Kim, G. Auchterlonie, J. Drennan, and J. H. Lee, *Sensors and Actuators B-Chemical*, 2008, **131**, 2.
19 J. Zeng, M. Hu, W. D. Wang, H. D. Chen, and Y. X. Qin, *Sensors and Actuators B-Chemical*, 2012, **161**, 1.
20 N. L. Wu, S. Y. Wang, and I. A. Rusakova, *Science*, 1999, **285**, 5432.
21 T. Sahm, L. Madler, A. Gurlo, N. Barsan, S. E. Pratsinis, and U. Weimar, *Sensors and Actuators B-Chemical*, 2004, **98**, 2.
22 G. L. Cui, M. Z. Zhang, and G. T. Zou, *Scientific Reports*, 2013, **3**, 1250.
23 J. S. Beveridge, M. R. Buck, J. F. Bondi, R. Misra, P. Schiffer, R. E. Schaak, and M. E. Williams, *Angewandte Chemie-International Edition*, 2011, **50**, 42.
24 D. E. Perea, N. Li, R. M. Dickerson, A. Misra, and S. T. Picraux, *Nano Letters*, 2011, **11**, 8.
25 W. I. Park, and G. C. Yi, *Advanced Materials*, 2004, **16**, 1.
26 S. P. Xu, F. Q. Sun, S. M. Yang, Z. Z. Pan, J. F. Long and F. L. Gu, *Scientific reports*, 2015, **5**, 8939.
27 F. Q. Sun, W. P. Cai, Y. Li, L. C. Jia and F. Lu, *Advanced Materials*, 2005, **17**, 23.
28 L. C. Jia, W. P. Cai, H. Q. Wang, F. Q. Sun and Y. Li, *ACS Nano*, 2009, **3**, 9.
29 M. D'Arienzo, L. Armelao, C. M. Mari, S. Polizzi, R. Ruffo, R. Scotti, and F. Morazzoni, *Journal of the American Chemical Society*, 2011, **133**, 14.

30 C. Yang, X. T. Su, F. Xiao, J. K. Jian, and J. D. Wang, *Sensors and Actuators B-Chemical*, 2011, **158**, 1.

31 P. Feng, X. Y. Xue, Y. G. Liu, and T. H. Wang, *Applied Physics Letters*, 2006, **89**. 24

32 S. Park, H. Ko, S. An, W. I. Lee, S. Lee, and C. Lee, *Ceramics International*, 2013, **39**, 5.

33 R. N. Mariammal, K. Ramachandran, G. Kalaiselvan, S. Arumugam, B. Renganathan, and D. Sastikumar, *Applied Surface Science*, 2013, **270**, 545.

34 P. Raksa, A. Gardchareon, T. Chairuangsri, P. Mangkorntong, N. Mangkorntong, and S. Choopun, *Ceramics International*, 2009, **35**, 2.

35 H. T. Hsueh, S. J. Chang, F. Y. Hung, W. Y. Weng, C. L. Hsu, T. J. Hsueh, S. S. Lin, and B. T. Dai, *Journal of the Electrochemical Society*, 2011, **158**, 4.

36 C. C. Huang, and C. S. Yeh, *Journal of Materials Science & Technology*, 2008, **24**, 4.

37 D. Gopalakrishna, K. Vijayalakshmi, and C. Ravidhas, *Ceramics International*, 2013, **39**, 7.

38 C. W. Na, S. Y. Bae, and J. Park, *Journal of Physical Chemistry B*, 2005, **109**, 12785.

39 J. Ghijsen, L. H. Tjeng, J. Vanelp, H. Eskes, J. Westerink, G. A. Sawatzky, and M. T. Czyzyk, *Physical Review B*, 1988, **38**, 16.

40 A. S. Zoolfakar, M. Z. Ahmad, R. A. Rani, J. Z. Ou, S. Balendhran, S. Zhuiykov, K. Latham, W. Wlodarski, and K Kalantar-Zadeh, *Sensors and Actuators B-Chemical*, 2013, **185**.

41 P. Q. Hu, G. J. Du, W. J. Zhou, J. J. Cui, J. J. Lin, H. Liu, D. Liu, J. Y. Wang, and S. W. Chen, *Acs Applied Materials & Interfaces*, 2010, **2**, 11.

42 Y. Shimizu, N. Nakashima, T. Hyodo, and M. Egashira, *Journal of Electroceramics*, 2001, **6**, 3.

43 C. W. Na, H.-S. Woo, I.-D. Kim, and J.-H. Lee, *Chemical Communications*, 2011, **47**, 18.

44 D. H. Yoon, J. H. Yu, and G. M. Choi, *Sensors and Actuators B*, 1998, **46**, 1.

